PHYSICAL REVIEW C VOLUME 25, NUMBER 1 JANUARY 1982

Neutron-proton decomposition of transition matrix elements from a comparison of 800 MeV proton scattering with electromagnetic methods

M. M. Gazzaly, N. M. Hintz, G. S. Kyle,* and R. K. Owen
University of Minnesota, Minneapolis, Minnesota 55455

G. W. Hoffmann
University of Texas, Austin, Texas 78712
and Los Alamos National Laboratory, Los Alamos, New Mexico 87545

M. Barlett
University of Texas, Austin, Texas 78712

G. Blanpied†
New Mexico State University, Las Cruces, New Mexico 88003
(Received 29 June 1981)

Differential cross sections for inelastic proton scattering at 800 MeV have been measured for a number of low-lying states in ^{90}Zr, ^{120}Sn, ^{144}Sm, and ^{208}Pb. The data from this and earlier experiments on ^{40}Ca and ^{58}Ni were analyzed with a collective vibrational model to obtain separate neutron and proton deformation lengths, making use of electromagnetic measurements. Ratios of neutron to proton transition matrix elements are calculated. These ratios are generally less than N/Z for the open proton shell nuclei and greater for the open neutron shell nuclei.

[NUCLEAR REACTIONS ^{90}Zr, ^{120}Sn, ^{144}Sm, ^{208}Pb(p,p'), $E=800$ MeV; measured $\sigma(\theta)$, $\theta_{lab}=5°-20°$. Optical model and DWBA collective model analysis. Deformation lengths and neutron to proton matrix element ratios are extracted for the above and ^{40}Ca, ^{58}Ni.]

I. INTRODUCTION

In the past few years, as a result of the availability of various intermediate energy probes, considerable progress has been made in the precision with which proton and neutron static, ground state density distributions could be determined. The most reliable methods seem to be either the comparison of π^+ with π^- scattering near the 3-3 resonance[1] or the use of charge densitites from electron scattering in the analysis of proton scattering near 1 GeV.[2] At present, the quoted errors in the densities extracted from electron-proton data are somewhat smaller than those from π^+- π^-. This reflects that (1) the electron and proton elastic data generally extend to higher momentum transfer than the pion data, and (2) theories of proton-nucleus scattering [Glauber, or Kerman, McManus, and Thaler (KMT)] seem at present more reliable than those for pion-nucleus. Given data and a theory of comparable quality, the two methods are about equally sensitive to neutron-proton differences (isovector densities).

The determination of neutron and proton *transition* densities can be made in the same way through a comparison of π^+ and π^- or of electron and proton scattering. High quality data exist on a number of inelastic cross sections for electron and proton scattering. It is the purpose of this paper to present some results on inelastic proton scattering at 800 MeV from ^{40}Ca, ^{58}Ni, ^{90}Zr, ^{120}Sn, ^{144}Sm, and ^{208}Pb, and to extract neutron and proton transition matrix elements from a comparison with electromagnetic measurements. In the analysis of the proton and electromagnetic data a simple vibrational model is used for the transition densities

together with a DWBA theory with relativistic kinematics for the proton scattering.

II. EXPERIMENTAL METHODS

The measurements reported here were done with the 800 MeV proton beam at the Los Alamos Clinton P. Anderson Meson Physics Facility (LAMPF), using the high resolution spectrometer (HRS). Isotopically enriched ($\geq 97\%$) targets of ^{90}Zr, ^{120}Sn, ^{144}Sm, and ^{208}Pb with areal densities ranging from 13 to 25 mg/cm^2 were used.

The beam intensity was monitored simultaneously by a set of ion chambers located inside the scattering chamber and by a set of two fixed three-fold coincidence monitor telescopes, which viewed the target at $\approx \pm 40°$ laboratory angles. At laboratory angles $\geq 12°$ a secondary emission monitor (SEM) located outside the scattering chamber, 3 m downstream of the target, was also used. Data were taken over the laboratory angular range of 5° to 20°, in steps of 1.5° to 2°. The angular resolution of the HRS as determined from the focal plane position and angle information was $\approx \pm 2$ mrad, while the accuracy of the spectrometer angle setting was measured to $\leq \pm 0.03°$. The beam energy was 800 ± 1 MeV.

During the off-line analysis the full horizontal acceptance of the spectrometer ($\approx 1.8°$) was divided into 4–5, 7-mrad (0.4°) bins, and the scattered events were sorted accordingly. The uncertainty in the scattering angle at the center of each bin was less than $\pm 0.03°$.

The peaks observed in the missing mass (excitation energy) spectra were fitted using the program LOAF[3] to obtain relative cross sections. Absolute cross sections were determined from the target areal densities (measured to $\pm 1\%$) and by comparing the ^{208}Pb$(p,p)^{208}$Pb elastic cross section measured during this experiment to the absolute measurements of Hoffmann *et al.*[4] The final cross sections are believed to be good to $\pm 5\%$. A detailed description of the data analysis technique is given in Ref. 4.

The overall energy resolution achieved was ≈ 100 keV, FWHM, for the ^{90}Zr, ^{120}Sn, and ^{144}Sm targets and 50–60 keV for ^{208}Pb (taken at a later date). Energy spectra for scattering from ^{90}Zr and ^{208}Pb are shown in Figs. 1 and 2. Differential cross sections for elastic and inelastic scattering are shown in Figs. 3–13. The errors shown in the figures are statistical only.

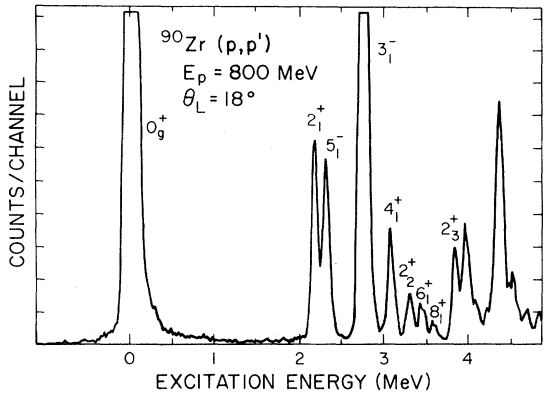

FIG. 1. Spectrum of 800 MeV protons scattered from ^{90}Zr at $\theta_L = 18°$.

III. DATA ANALYSIS

A. Elastic scattering

The elastic cross sections were analyzed using the optical model code RELOM,[5] with relativistic kinematics and a Woods-Saxon potential of the form

$$U_{\text{opt}}(r) = V_0 f(x) - iW_0 f(x') + V_c \ ,$$

where

$$f(x) = (1+e^x)^{-1} \ , \quad f(x') = (1+e^{x'})^{-1} \ ,$$

and

$$x = (r - R_r)/a_r \ , \quad x'(r - R_I)/a_I \ , \tag{1}$$

with

$$R_r = r_{0r} A^{1/3}$$

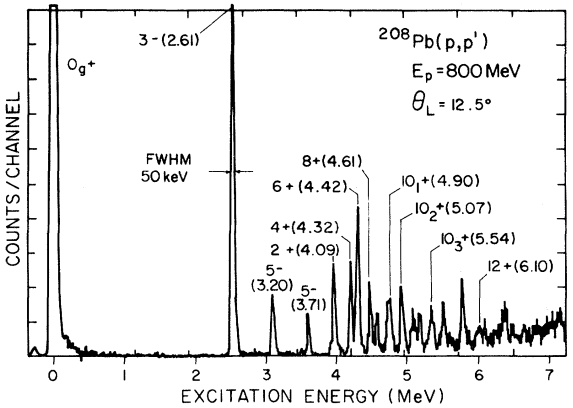

FIG. 2. Spectrum of 800 MeV protons scattered from ^{208}Pb at $\theta_L = 12.5°$.

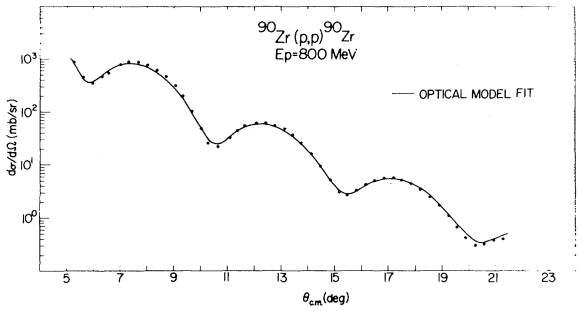

FIG. 3. Elastic differential cross sections for ^{90}Zr at $E_p = 800$ MeV. Solid curve is optical model prediction.

and

$$R_I = r_{0I} A^{1/3} .$$

V_c is the Coulomb potential for a uniformly charged sphere of radius $r_c = 1.049A^{1/3}$. For ^{90}Zr, ^{120}Sn, and ^{208}Pb the geometric constraint $x = x'$ was used and the parameters V_0, W_0, r_0, and a_0 determined by searching on the data. In the case of ^{144}Sm the constraint $x = x'$ was not used. For ^{208}Pb, the free search on the geometry and strength parameters led to values of r_0 and a_0 (set I) which gave a value of $\langle r^2 \rangle_w^{1/2} = 5.396$ fm for the rms radius of the imaginary potential. Since the deduced point mass densities for ^{208}Pb were found to be[4] $\langle r^2 \rangle_p^{1/2} = 5.453$ fm and $\langle r^2 \rangle_n^{1/2} = 5.593$ fm, which are somewhat larger than the above $\langle r^2 \rangle_W^{1/2}$, another search (set II) was made constraining the potential moment to $\langle r^2 \rangle_W^{1/2} = 5.588$ fm, the value expected from the deduced matter densities for a potential obtained by folding. The fits to the data were essentially the same for the two potentials, as were the deformation lengths obtained. The calculated optical model cross sections are shown with

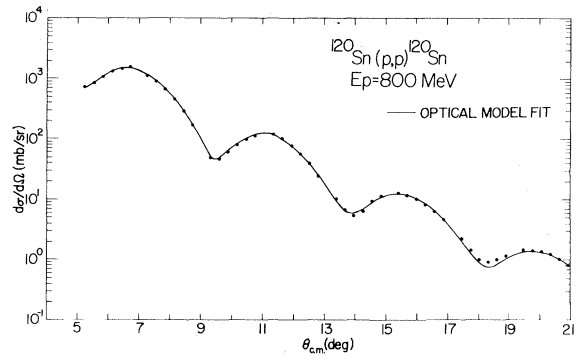

FIG. 4. Elastic differential cross sections for ^{120}Sn at $E_p = 800$ MeV. Solid curve is optical model prediction.

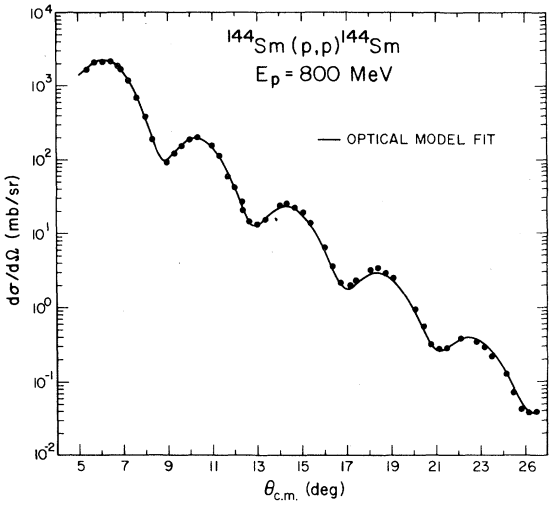

FIG. 5. Elastic differential cross sections for ^{144}Sm at $E_p = 800$ MeV. Solid curve is optical model prediction.

the elastic data in Figs. 3—6. The optical parameters are given in Table I.

B. Inelastic scattering

The inelastic cross sections were analyzed using the collective vibrational model[6] in the DWBA program CHORK[7] with relativistic kinematics. The radial part of the interaction potential for exciting a multipole vibration (λ) is thus,

$$V_\lambda = \delta_U \frac{\partial U_{\text{opt}}}{\partial r} , \tag{2}$$

where

$$\delta_U = (\beta_\lambda R_0)_U ,$$

the potential U_{opt} having been fixed in the elastic

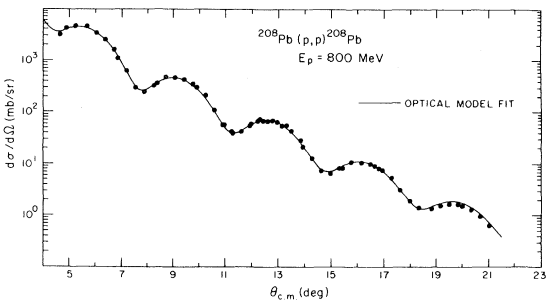

FIG. 6. Elastic differential cross sections for ^{208}Pb at $E_p = 800$ MeV. Solid curve is optical model (set II) prediction.

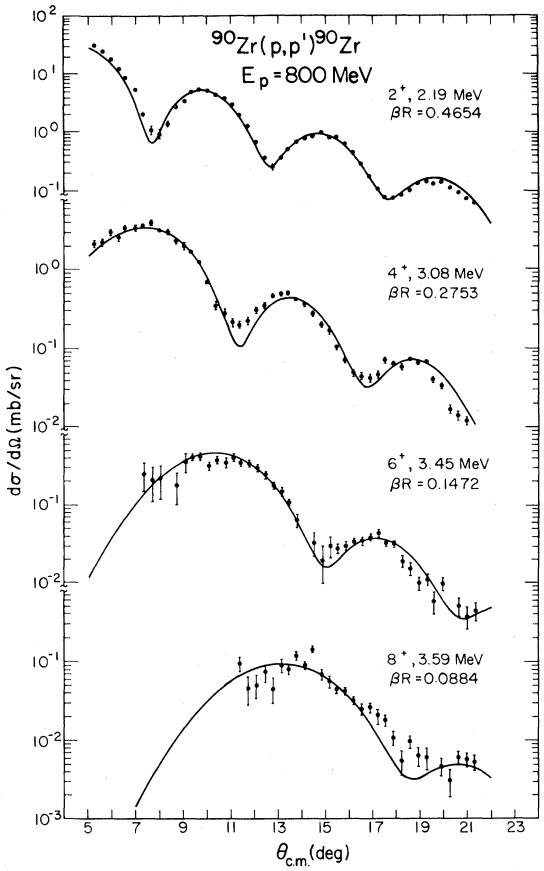

FIG. 7. Inelastic cross sections for ^{90}Zr at $E_p = 800$ MeV. Solid lines are DWBA predictions.

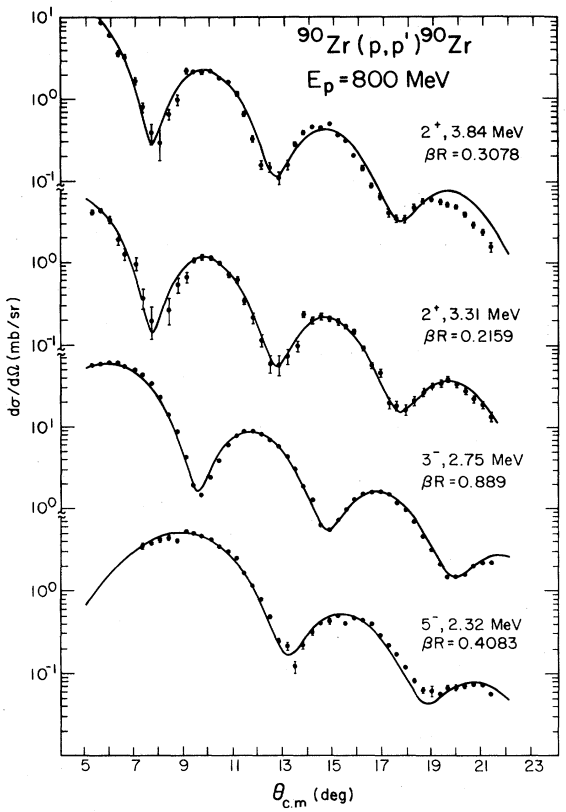

FIG. 8. Inelastic cross sections for ^{90}Zr at $E_p = 800$ MeV. Solid lines are DWBA predictions.

analysis. In this model the excited states of spin I are assumed to be one phonon surface vibrations of order $\lambda = I$. The resultant inelastic predictions are shown in Figs. 7—13 with the data.

The agreement between calculated cross sections and the data is remarkable except for the 3_1^- state of ^{120}Sn, which was not fully resolved. Unlike the situation frequently encountered with lower energy hadronic probes, the fits to the angular distributions were sufficiently good over several diffraction maxima that no ambiguities arose in normalizing theory to experiment to obtain the deformation lengths δ_U.

The sensitivity of the deformation lengths to the absolute normalization of the data was explored by varying the experimental cross sections by 10%, and then searching on the renormalized elastic data to find new optical parameters. The resulting deformation lengths were found to change by only 2—3%. The two ^{208}Pb optical parameter sets (I and II of Table I) gave values for δ_U differing by

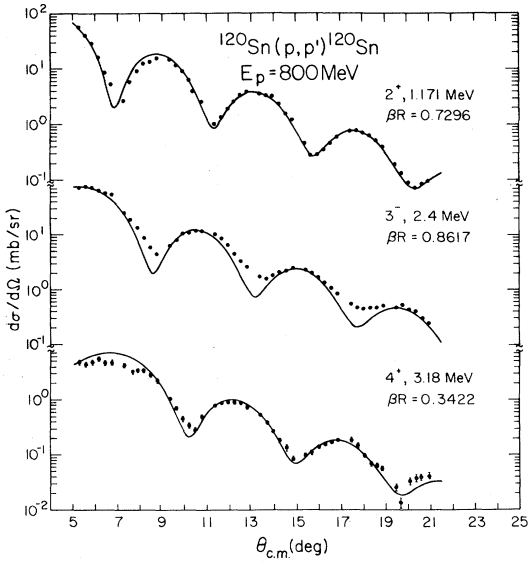

FIG. 9. Inelastic cross sections for ^{120}Sn at $E_p = 800$ MeV. Solid lines are DWBA predictions.

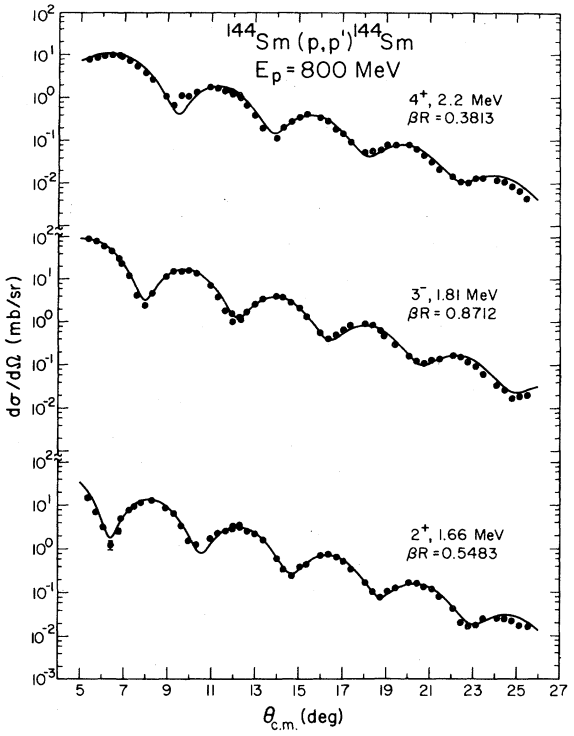

FIG. 10. Inelastic cross sections for ^{144}Sm at $E_p = 800$ MeV. Solid lines are DWBA predictions.

$\lesssim 3\%$. Thus, it is believed that our values of δ_U are determined to better than 5%. The deformation lengths obtained from this experiment are given in Table II, along with values for ^{40}Ca and ^{58}Ni from earlier 800 MeV (p,p') analyses.[8,9]

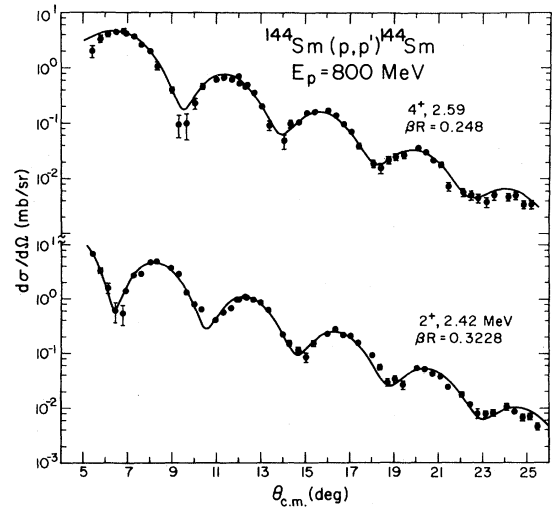

FIG. 11. Inelastic cross sections for ^{14}Sm at $E_p = 800$ MeV. Solid lines are DWBA predictions.

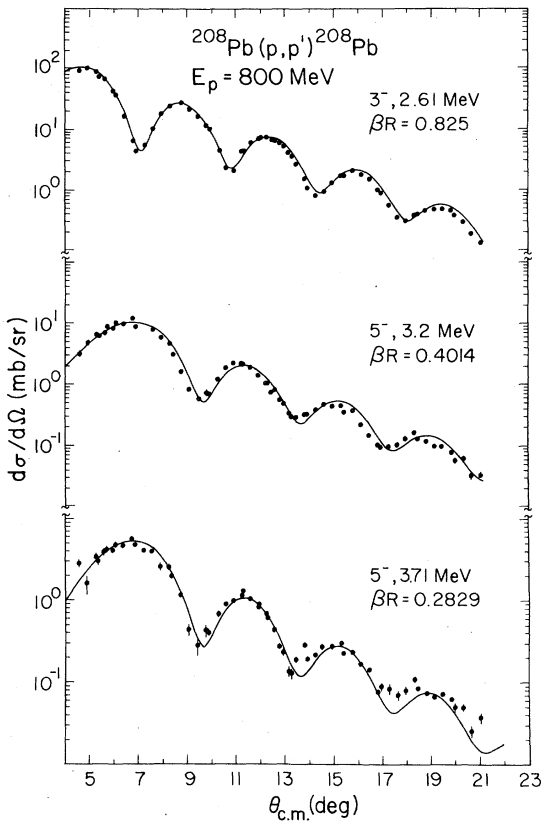

FIG. 12. Inelastic cross sections for ^{208}Pb at $E_p = 800$ MeV. Solid lines are DWBA predictions.

IV. NEUTRON-PROTON DECOMPOSITION OF TRANSITION MATRIX ELEMENTS

The analysis performed here follows the methods of Bernstein[10] and Madsen *et al.*[10] with the following exceptions. We do not assume that the neutron (ρ_n) and proton (ρ_p) densities have the same radial moments. Also, we distinguish between charge (ρ_q) and point proton (ρ_p) densities.

Since the deformation lengths δ_i (i: U, n, p, or q) represent displacements of the corresponding equidensity surfaces, we make the same assumptions as Bernstein, namely,

$$\delta_p = \delta_q \ , \qquad \delta_{U_p} = \delta_p \ , \tag{3}$$

and

$$\delta_{U_n} = \delta_n \ , \tag{4}$$

where δ_{U_n} and δ_{U_p} are deformation lengths for those parts of the potentials generated by the target

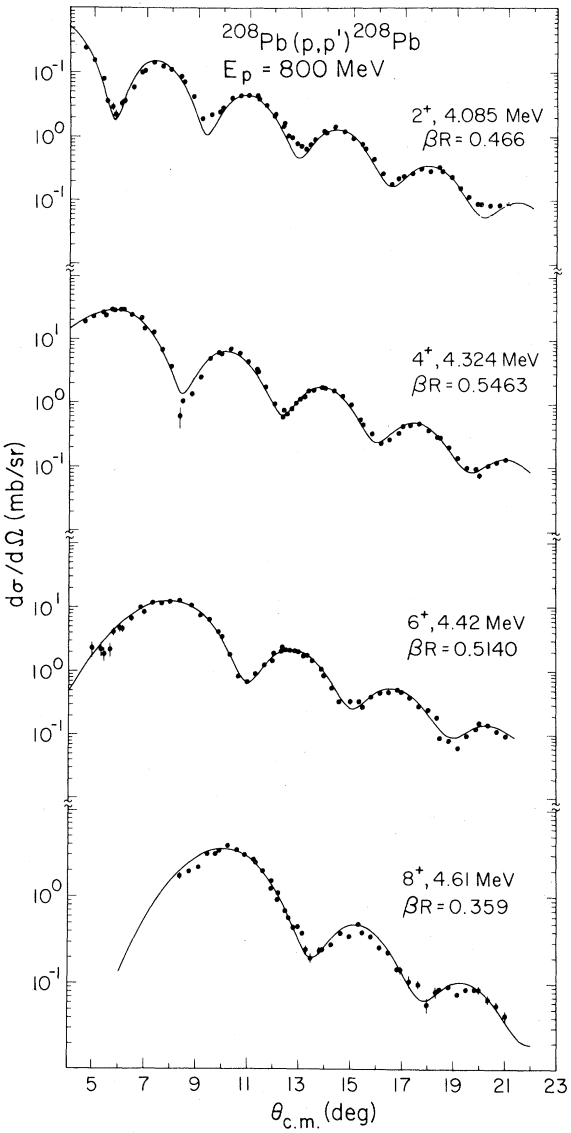

FIG. 13. Inelastic cross sections for ^{208}Pb at $E_p=800$ MeV. Solid lines are DWBA predictions.

neutrons and protons, respectively, and δ_n and δ_p are the point density deformation lengths. These relations are strictly true only in the limit $R \gg d$, where R is the nuclear radius and d is the range of the projectile-nucleon force (or the size of the proton charge distribution in the case of $\rho_p=\rho_q$).

The approximations of Eq. (4), equating potential and density displacements, are expected to be considerably better for 800 MeV protons than for lower energy hadronic probes, since (1) the 800 MeV potentials are approximately linear in the densities (validity of first-order KMT theory), and (2) the rms radius of the effective two-body force ($\langle r^2\rangle_d^{1/2}\simeq 0.8$ fm) is considerably smaller than at low energy.

The separation into target neutron and proton components is done as follows. We assume the optical potential can be written

$$U_{\text{opt}}=U_n+U_p \ , \tag{5}$$

which is valid in first order KMT (neglecting correlations). Then,

$$\frac{\partial U_{\text{opt}}}{\partial r}=\frac{\partial U_n}{\partial r}+\frac{\partial U_p}{\partial r} \ . \tag{6}$$

The interaction potential used in the collective model calculations, V_γ, is then assumed to be

$$V_\lambda=\delta_U\frac{\partial U_{\text{opt}}}{\partial r}\cong\delta_n\frac{\partial U_n}{\partial r}+\delta_p\frac{\partial U_p}{\partial r} \ . \tag{7}$$

Thus, V_γ represents the best approximation to the sum of the separate neutron and proton terms.

Now, since

$$\rho_n/N\simeq\rho_p/Z \ , \tag{8}$$

and, since the imaginary central, spin independent part of the nucleon-nucleon force at 800 MeV (which dominates in the optical potential) is almost purely isoscalar, then

$$\frac{1}{N}\frac{\partial U_n}{\partial r}\simeq\frac{1}{Z}\frac{\partial U_p}{\partial r} \ . \tag{9}$$

We can thus expand about the approximations of Eqs. (8) and (9) and write

$$\delta_U=\delta_0+\delta_1\frac{U_n'-U_p'}{U_n'+U_p'} \ , \tag{10}$$

where

$$\delta_0=\frac{\delta_n+\delta_p}{2}$$

and

$$\delta_1=\frac{\delta_n-\delta_p}{2} \ .$$

The primes denote differentiation with respect to r.

Then, letting $\epsilon=(N-Z)/A$, Eq. (10) can be written

$$\delta_U=\delta_0+\delta_1\frac{\epsilon+K}{1+\epsilon K} \ , \tag{11}$$

where

$$K=\frac{1-\nu}{1+\nu}$$

and

TABLE I. Optical model parameters.[a]

Nucleus	V_0 (MeV)	r_{or} (fm)	a_r (fm)	W_0 (MeV)	r_{oI} (fm)	a_I (fm)	$\langle r^2\rangle_w^{1/2}$ (fm)	$\langle r^2\rangle_\rho^{1/2}$ [c] (fm)
^{40}Ca[b]	4.40	0.89	0.69	66.6	1.01	0.61	3.507	3.497
^{58}Ni[b]	6.33	0.977	0.689	64.2	1.047	0.580	3.808	3.701
^{90}Zr	9.38	1.038	0.589	83.4	1.038	0.589	4.217	4.254
^{120}Sn	6.03	1.046	0.621	83.1	1.046	0.621	4.615	4.677
^{144}Sm	4.73	1.076	0.970	76.8	1.073	0.623	4.934	4.914
^{208}Pb I	6.12	1.047	0.661	97.3	1.047	0.661	5.396	5.535
^{208}Pb II[d]	7.72	1.117	0.599	60.2	1.117	0.599	5.588	5.535

[a]Standard Woods-Saxon potential with volume absorption [Eq. (1), text]. V_0 is repulsive.
[b]From Ref. 8 (^{40}Ca) and Ref. 9 (^{58}Ni). A spin-orbit potential was included in these analyses.
[c]$\langle r^2\rangle_\rho^{1/2}=[(1/A)\ (Z\langle r^2\rangle_p+N\langle r^2\rangle_n)]^{1/2}$.
[d]$\langle r^2\rangle_w^{1/2}$ constrained to 5.588 fm in search.

$$\nu=\frac{U_p' N}{U_n' Z}\ .$$

In order to evaluate the coefficient, δ_1 of the isovector part of the deformation length in Eq. (11), one needs to calculate K. This requires the knowledge of ν, which is a function of radius. Thus, one is required to choose same average value $\langle\nu\rangle$ for ν.

Since $\langle K\rangle\simeq -0.1$ for 800 MeV protons, our results are insensitive to the method of estimating $\langle\nu\rangle$. We choose to use the volume integrals of U_n' and U_p' to evaluate $\langle\nu\rangle$.

We define the volume integral of a function $h(r)$ as

$$J_0(h)=\int h(r)d^3r\ . \tag{12}$$

In first order KMT the potentials are given by

$$U_i=\int \rho_i(r')g_i(\,|\,r-r'\,|\,)d^3r'\quad (i=n \text{ or } p)\ , \tag{13}$$

where g_i is the projectile-nucleon force. Then, using the volume integral theorem of Satchler,[11]

$$J_0(U_i)=J_0(\rho_i)J_0(g_i)=(N \text{ or } Z)J_0(g_i) \tag{14}$$

and writing $U_i(r)=V_i f_i(r)$, where V_i is a constant, we obtain

$$\langle\nu\rangle=\frac{NJ_0(U_p')}{ZJ_0(U_n')}=\frac{J_0(g_p)J_0(f_p')J_0(f_n)}{J_0(f_p)J_0(g_n)J_0(f_n')}\ . \tag{15}$$

The volume integrals of g_n and g_p are taken from the central, spin-independent part of the Love-Franey force,[12] for which

$$J_0(g_p)/J_0(g_n)=1.197\ .$$

The potential volume integrals $J_0(f_i)$ and $J_0(f_i')$ are calculated using two parameter Fermi distributions which reproduce the half value and surface thickness generated by folding the neutron and proton point densities of Ray, Coker, and Hoffmann,[2] Hoffmann *et al.*,[4] and Ray[13] with a two-body force of range $\langle r^2\rangle_d^{1/2}=0.79$ fm, the approximate effective force range found for the KMT potentials. The values of

$$\langle\nu\rangle\ ,\ K,\ \text{and}\ \tilde{K}=\frac{\epsilon+K}{1+\epsilon K}$$

are given in Table III.

To obtain neutron and proton deformation lengths and transition matrix elements, we assume the simple surface vibrational model for which the transition density is given by

$$\rho_{\rm tr}^{(i)}=\delta_i\frac{\partial\rho_i}{\partial r}\quad (i:\ n,\ p,\ \text{or}\ q)\ . \tag{16}$$

The reduced (N or Z factors removed) transition matrix element $\tilde{M}_i(\lambda)$ is then given by

$$\tilde{M}_i(\lambda)=\frac{1}{N \text{ or } Z}\int\rho_{\rm tr}^{(i)}r^{\lambda+2}dr$$
$$=\left[\frac{\lambda+2}{4\pi}\langle r^{\lambda-1}\rangle_i\delta_i\right]\ . \tag{17}$$

We further make the assumptions of Eqs. (3) and (4), relating charge (q), potential (U), and matter density (n, p) deformation lengths.

In this model the reduced electromagnetic transition probability is given by (assuming $\delta_q=\delta_p$)

TABLE II. Proton and neutron deformation lengths and matrix elements. See text for explanation of symbols.

Nucleus	J^π	E (MeV)	δ_U (fm)	δ_p[a] (fm)	δ_n (fm)	$B(p,\lambda)$ (b^λ)	$B(E\lambda)$[b] (e^2b^λ)	$\tilde{M}_n/\tilde{M}_p$	M_n/M_p
^{40}Ca[c]	3_1^-	3.74	1.39	1.40(5)	1.38(6)	0.0180	0.0182(13)	0.99(8)	0.99(8)
	2_1^+	3.90	0.52	0.48(5)	0.57(6)	0.0118	0.0100(20)	1.2(2)	1.2(2)
	5_1^-	4.49	0.76	0.74(5)	0.79(6)	3.25×10^{-4}	$3.1(4)\times10^{-4}$	1.06(15)	1.06(15)
^{58}Ni	2_1^+	1.46	0.902	0.82(2)	0.99(2)	0.0823	0.0685(30)	1.20(5)	1.29(5)
	3_1^-	4.48	0.778	0.83(5)	0.73(5)	0.0153	0.0171(19)	0.89(11)	0.95(12)
	4_1^+	2.46	0.403	0.39(6)	0.41(7)	0.00105	0.0010(3)	1.07(34)	1.15(37)
	2_3^+	3.04	0.270	0.29(1)	0.25(1)	0.00741	0.0083(3)	0.88(4)	0.95(4)
	2_4^+	3.26	0.37	0.40(4)	0.34(5)	0.0139	0.016(3)	0.86(20)	0.92(21)
^{90}Zr	2_1^+	2.19	0.465	0.495(8)	0.437(8)	0.0581	0.0661(21)	0.90(13)	1.12(4)
	3_1^-	2.75	0.889	0.98(2)	0.80(2)	0.0667	0.082(4)	0.85(4)	1.06 (5)
	5_1^-	2.32	0.408	0.51(3)	0.31(3)	0.00168	0.0027(3)	0.65(9)	0.81(12)
	4_1^+	3.08	0.275	0.35(2)	0.21(2)	0.00215	0.0035(4)	0.62(10)	0.78(12)
	2_2^+	3.31	0.216	0.171(8)	0.259(8)	0.0126	0.0079(8)	1.54(12)	1.93(16)
	6_1^+	3.45	0.147	0.20	0.093	8.2×10^{-5}	1.62×10^{-4}	0.50	0.63
	8_1^+	3.59	0.0884	0.13	0.050	5.0×10^{-6}	1.11×10^{-5}	0.45	0.56
	2_3^+	3.84	0.308	0.30(1)	0.316(10)	0.0255	0.0243(16)	1.07(7)	1.34(9)
^{120}Sn	2_1^+	1.17	0.730	0.633(5)	0.814(5)	0.266	0.200(3)	1.33(2)	1.87(3)
	3_1^-[c]	2.40	0.862	0.77(7)	0.94(6)	0.137	0.11(2)	1.3(2)	1.84(3)
	4^+[c]	3.18	0.342						
^{144}Sm	2_1^+	1.66	0.548	0.550(12)	0.547(11)	0.260	0.262(11)	1.00(4)	1.32(5)
	3_1^-	1.81	0.871			0.276			
	4_1^+	2.19	0.381			0.0236			
	2_2^+	2.42	0.323			0.903			
	4_2^+	2.59	0.248			0.00999			
^{208}Pb	3_1^-	2.61	0.825	0.798(10)	0.847(8)	0.664	0.621(16)	1.12(3)	1.72(4)
	5_1^-	3.20	0.401	0.395(13)	0.407(11)	0.0463	0.0447(30)	1.18(7)	1.81(11)
	5_2^-	3.71	0.283	0.290(11)	0.278(9)	0.0230	0.0241(18)	1.10(7)	1.68(12)
	2_1^+	4.09	0.466	0.409(10)	0.511(8)	0.412	0.318(16)	1.28(5)	1.97(8)
	4^+	4.32	0.546	0.546(18)	0.546(14)	0.155	0.155(10)	1.10(6)	1.69(10)
	6_1^+	4.42	0.514	0.635(32)	0.418(25)	0.0436	0.0665(67)	0.79(9)	1.22(13)
	8_1^+	4.61	0.359	0.298(25)	0.408(20)	0.00786	0.0054(9)	1.87(25)	2.87(38)

[a]Calculated from $B(E\lambda)$ of column 8.
[b]$B(E\lambda)$ references given in Table IV.
[c]States not fully resolved.

$$B(E\lambda)=|Z\tilde{M}_q(\lambda)|^2 = \left[\frac{Z(\lambda+2)}{4\pi}\langle r^{\lambda-1}\rangle_q\delta_p\right]^2 . \quad (18)$$

The procedure used in this analysis is to calculate δ_p from Eq. (18) using the best available (or weighted average) of the electromagnetic transition rates $B(E\lambda)$, together with a value of $\langle r^{\lambda-1}\rangle_q$ calculated from electron scattering charge densities.[14] The $B(E\lambda)$'s found in the literature are given in Table IV, and the adopted values are given in Tables II and IV. Equations (11) and (15) are then used to obtain δ_n. The values obtained for δ_p and δ_n are given in Table II. Also in Table II, we have, for comparison with the adopted $B(E\lambda)$'s, tabulated the quantity "$B(p,\lambda)$," defined as

$$B(p,\lambda)=\left[\frac{Z(\lambda+2)}{4\pi}\langle r^{\lambda-1}\rangle_q\delta_U\right]^2 . \quad (19)$$

Here we have used the total potential deformation length δ_U from the DWBA analysis together with

TABLE III. Parameters used in decomposition of matrix elements.

	^{40}Ca	^{58}Ni	^{90}Zr	^{120}Sn	^{144}Sm	^{208}Pb
ν	1.197	1.200	1.207	1.212	1.21	1.216
K	−0.0896	−0.0909	−0.0937	−0.0958	−0.0948	−0.0975
$\tilde{K}$	−0.0896	−0.0566	0.0176	0.0720	0.0447	0.116
$\langle r^n\rangle_n$ $n=1$	3.276	3.507	4.102	4.542	4.702	5.362
(fm^n) 2	12.23	13.73	18.40	22.56		31.29
3		58.71	88.27			194.3
4	229.8		447.1			1267
5			2373			8626
7			75 579			445 709
$\langle r^n\rangle_p$ $n=1$	3.276	3.508	4.022	4.379	4.662	5.233
(fm^n) 2	12.23	13.66	17.76	20.91		29.63
3		57.70	83.55			177.3
4	229.8		415.8			1107
5			2168			7169
7			66 498			326 688
$\langle r^n\rangle_q$ $n=1$	3.284	3.576	4.079	4.442	4.716	5.280
(fm^n) 2	12.12	14.17	18.35	21.58		30.27
3		60.67	88.81			184.1
4	212.8		455.9			1173
5			2462			7780
7			81 883			378 459

the charge moment. This quantity should be equal to $B(E\lambda)$ if $\delta_p=\delta_n$ ($\delta_1=0$). The last two columns of Table II give the ratio of the neutron and proton transition matrix elements calculated from Eq. (17), i.e.,

$$\tilde{M}_n/\tilde{M}_p=\frac{\langle r^{\lambda-1}\rangle_n\delta_n}{\langle r^{\lambda-1}\rangle_p\delta_p} \tag{20}$$

and $M_n/M_p=N/Z\tilde{M}_n/\tilde{M}_p$.

The moments $\langle r^{\lambda-1}\rangle_{n,p}$ were calculated from the point densities of Ray, Coker, and Hoffmannn,[2] Hoffman *et al.*,[4] and Ray[3] obtained from electron scattering charge densities and 800 MeV proton scattering. Generally, the best fit three-parameter Gaussians from the above analysis were used to calculate $\langle r^{\lambda-1}\rangle$. The quantity $\tilde{M}_n/\tilde{M}_p$ should be unity if the transition is purely isoscalar. The ratio of the neutron to proton radial moments, $\langle r^{\lambda-1}\rangle_n/\langle r^{\lambda-1}\rangle_p$, was taken to be unity for ^{40}Ca, but is calculated to be 1.06 ($\lambda=3$) and 1.36 ($\lambda=8$) for ^{208}Pb. It should be noted that the three-parameter Gaussian representations of ρ_n and ρ_p are probably increasingly unreliable for $\lambda>5$ (r^4 moments). The calculated moments $\langle r^n\rangle_i$ are given in Table III.

The errors given in Table II represent only those due to the error in the adopted value of $B(E\lambda)$. These are generally larger than what we believe to be the uncertainty in δ_U from this experiment. In our analysis of the new data presented here we have omitted the spin-orbit term in both the diagonal (elastic) and off-diagonal (inelastic) potentials. The deformation lengths obtained for spherical nuclei, when the spin-orbit terms are neglected, have been shown[15] to be within 2−3 % of those obtained when it is included, provided the optical potential is adjusted to recover the fit to the elastic cross sections. This is true at least at 800 MeV, where the spin-orbits force is relatively weak, and for low spin ($I\lesssim 4$) states. Similarly, coupled-channels effects on δ_U are found[16] to be small ($\lesssim$2−3 %) for states in single closed shell nuclei that are well described by the collective form factors used here. The worst case, of those presented here, is the 4_1^+ ("two-phonon") state of ^{58}Ni, where the direct one step deformation length obtained in the DWBA is reduced by 10% when a coupled-channels analysis[16] is made.

TABLE IV. $B(E\lambda)$ values.

Nucleus	J^π	E_{ex} (MeV)	$B(E\lambda)$ (e^2b^λ)	Method	Ref.
^{40}Ca	3_1^-	3.74	0.0204(17)	lifetime	Ta72c[a]
			0.0211(30)	(e,e')	Ei69a[a]
			0.0166(7)	(e,e')	b
			0.0149(7)	(e,e')	Ha73b[a]
			0.0182(7)	(e,e')	It70[a]
			0.0235(10)	(e,e')	c
			0.0182(13)	adopted	
	2_1^+	3.90	0.0085(10)	lifetime	d
			0.0081(8)	(e,e')	Ei69a[a]
			0.0090(10)	(e,e')	Ha73b[a]
			0.0122(8)	(e,e')	It70[a]
			0.0118(8)	(e,e')	c
			0.0100(20)	adopted	
	5_1^-	4.49	$1.62(10)\times10^{-4}$	(e,e')	b
			$3.38(100)\times10^{-4}$	(e,e')	It70[a]
			$3.00(15)\times10^{-4}$	(e,e')	c
			$3.1(4)\times10^{-4}$	adopted	
^{58}Ni	2_1^+	1.46	0.064(5)	lifetime	e
			0.072(7)	CE	62St02[e]
			0.0726(20)	CE	70Le17[e]
			0.066(4)	CE	73Ch13[e]
			0.099(13)	(e,e')	61Cr01[e]
			0.0657(11)	(e,e')	67Du07[e]
			0.055(3)	(e,e')	69Af01[e]
			0.0685(30)	adopted	
	3_1^-	4.48	0.027(4)	(e,e')	61Cr01[e]
			0.0186(5)	(e,e')	67Du07[e]
			0.0130(8)	(e,e')	69Af01[e]
			0.0171(19)	adopted	
	4_1^+	2.46	0.0010(3)	(e,e')	61Cr01[e]
	2_3^+	3.04	0.0083(3)	(e,e')	67Du07[e]
	2_4^+	3.26	0.016(2)	lifetime	e
			0.031(7)	(e,e')	61Cr01[e]
			0.0153(15)	(e,e')	67Du07[e]
			0.016(3)	adopted	
^{90}Zr	2_1^+	2.19	0.0608(35)	(γ,γ')	72Me04[f]
			0.0673(59)	(e,e')	g
			0.0661(21)	(e,e')	h
			0.0661(21)	adopted	
	3_1^-	2.75	0.108(3)	(e,e')	70Be07[f]
			0.0801(?)	(e,e')	73Ph02[f]
			0.0874(100)	(e,e')	g
			0.0819(36)	(e,e')	h
			0.0819(36)	adopted	

TABLE IV. (*Continued.*)

Nucleus	J^π	E_{ex} (MeV)	$B(E\lambda)$ (e^2b^λ)	Method	Ref.
	5_1^-	2.32	0.00212(12)	(e,e')	g
			0.00289(32)	(e,e')	h
			0.0027(3)	adopted	
	4_1^+	3.08	0.00295(80)	(e,e')	g
			0.00348(40)	(e,e') adopted	h
	2_2^+	3.31	0.0069(18)	(e,e'), $(\gamma\gamma')$	g
			0.0079(8)	(e,e'), adopted	h
	6_1^+	3.45	1.62×10^{-4}	(e,e')	h
	8_1^+	3.59	1.11×10^{-5}	(e,e')	h
	2_3^+	3.84	0.0206(36)	(e,e'), (γ,γ')	g
			0.0243(16)	(e,e'), adopted	h
^{120}Sn	2_1^+	1.17	0.203(4)	CE	70St20[i]
			0.197(4)	CE	j
			0.12(2)	(e,e')	67Ba52[i]
			0.23 – 0.17	(e,e')	69Cu06[i]
			0.200(3)	adopted	
	3_1^-		0.13(5)	CE	69Al26[i]
			0.10 – 0.15	(e,e')	69Cu06[i]
			0.11(1)	(e,e')	67Ba52[i]
			0.11(2)	adopted	
^{144}Sm	2_1^+		0.39(12)	CE	63Al31[k]
			0.25(4)	CE	66Ec02[k]
			0.262(6)	CE	l
			0.262(11)	adopted	
^{208}Pb	3_1^-	2.61	0.64(4)	CE	m
			0.60(7)	CE	n
			0.665(35)	CE	o
			0.66(5)	CE	p
			0.54(3)	lifetime	q
			0.612(14)	(e,e')	r
			0.624(40)	(e,e')	s
			0.621(16)	adopted	
	5_1^-	3.20	0.053(15)	(e,e')	s
			0.0451(57)	(e,e')	t
			0.0447(30)	(e,e')	u
			0.0447(30)	adopted	
	5_2^-	3.71	0.0325(81)	(e,e')	t
			0.0217(27)	(e,e')	s
			0.0241(18)	(e,e')	u
			0.0241(18)	adopted	

TABLE IV. (*Continued.*)

Nucleus	J^π	E_{ex} (MeV)	$B(E\lambda)$ (e^2b^λ)	Method	Ref.
^{208}Pb	2_1^+	4.09	0.30(2)	(e,e')	t,v
			0.247(30)	(e,e')	w
			0.318(16)	(ee')	u
			0.318(16)	adopted	
	4_1^+	4.32	0.23(2)	(ee')	v
			0.204(40)	(ee')	w
			0.129(20)	(ee')	t
			0.155(10)	(ee')	u
			0.155 (10)	adopted	
	6_1^+	4.42	0.0422(80)	(e,e')	w
			0.0665(67)	(e,e')	u
			0.0665(67)	adopted	
	8_1^+	4.61	0.0098(30)	(e,e')	w
			0.0054(9)	(e,e')	u
			0.0054(9)	adopted	

[a]References quoted in P. M. Endt and C. VanDer Leuen, Nucl. Phys. A310, 533 (1978).
[b]J. Heisenberg, J. S. McCarthy, and I. Sick, Nucl. Phys. A164, 353 (1971).
[c]K. Seth, private communication.
[d]Based on weighted average lifetimes from references quoted in Ref. a.
[e]References quoted in D. C. Kocher and R. L. Auble, Nucl. Data Sheets 19, 445 (1976).
[f]Reference quoted in D. C. Kocher, Nucl. Data Sheets 16, 55 (1975).
[g]R. P. Singhal *et al.*, J. Phys. G 1, 588 (1975). Earlier data included in analysis.
[h]J. Heisenberg, private communication. Analysis includes new data and all earlier data.
[i]References quoted in D. C. Kocher, Nucl. Data Sheets 17, 39 (1976).
[j]R. Graetzer, S. M. Cohick, and J. K. Saladin, Phys. Rev. C 12, 1462 (1975).
[k]References quoted in J. K. Tuli, Nucl. Data Sheets 27, 97 (1979).
[l]G. Kindleben and Th. W. Elze, Z. Phys. A 286, 415 (1978).
[m]Reanalysis of data from A. R. Barnett and W. R. Phillips, Phys. Rev. 186, 1205 (1969) by authors.
[n]E. Grosse *et al.*, Nucl. Phys. A174, 525 (1971).
[o]A. M. R. Joye *et al.*, Phys. Rev. Lett. 38, 807 (1977).
[p]J. S. Lilley, M. A. Franey, and D. A. Hsuan Feng, Nucl. Phys. A342, 165 (1980).
[q]O. Hausser, F. C. Khanna, and D. Ward, Nucl. Phys. A194, 113 (1972).
[r]D. Goutte *et al.*, Phys. Rev. Lett. 45, 1618 (1980).
[s]J. Freidrich, Nucl. Phys. A191, 118 (1972).
[t]M. Nagao and Y. Torizuka, Phys. Lett. 37B, 383 (1971).
[u]J. Lichtenstadt, Ph. D. thesis, MIT, 1979 (unpublished); J. Heisenberg, private communication. Later analysis (J. H.) includes data of Ref. s.
[v]J. F. Ziegler and G. A. Peterson, Phys. Rev. 165, 1337 (1968).
[w]E. Weber, W. Knüpfer, E. Grecksch, M. G. Huber, Phys. Lett. 65B, 189 (1976); analysis of data of J. Friedrich, N. Voegler, and H. Euteneuer, Phys. Lett. 64B, 269 (1976).

V. CONCLUSIONS

The values of the reduced (N and Z factors removed) matrix element ratios $\tilde{M}_n/\tilde{M}_p$ in Table II generally show the expected[10] behavior for the low lying 2_1^+ and 3_1^- collective states. For the open neutron shell nuclei (^{58}Ni, ^{120}Sn), $\tilde{M}_n/\tilde{M}_p > 1$, except for the 3_1^- state of ^{58}Ni.

A determination of the ratios δ_n/δ_p for the 2_1^+ and 3_1^- states of ^{58}Ni from π^+ and π^- inelastic scattering[17] gives $\delta_n/\delta_p = 1.21 \pm 0.14$ for the 2_1^+ state, in excellent agreement with our value of 1.205 ± 0.05. The π^+-π^- result for the 3_1^- state is $\delta_n/\delta_p = 1.22 \pm 0.15$, which is a more realistic value than our (0.88 ± 0.11). However, the three $B(E3)$ values obtained from electron scattering are in seri-

ous disagreement with each other (see Table IV).

Conversely, the open proton shell nucleus ^{90}Zr shows $\tilde{M}_n/\tilde{M}_p < 1$ for the four lowest states. For ^{144}Sm (open protons) only the 2_1^+ state has a measured $B(E\lambda)$ and for this case $\tilde{M}_n/\tilde{M}_p = 1.0$ which is unexpected.

The nuclei ^{40}Ca and ^{208}Pb provide test cases for our methods. Isospin conservation implies $M_n/M_p = 1$ for ^{40}Ca, as is obtained here within the errors of the measured $B(E\lambda)$'s. A recent ^{40}Ca $(\pi^{\pm},\pi^{\pm'})$ comparision[18] gives $M_n/M_p = 1.0 \pm 0.06$ for the 3_1^- and 2_1^+ states, in agreement with our results. In the case of ^{208}Pb there is evidence from the comparison of low energy (α,α') scattering with electromagnetic methods[19] that the 3_1^- state is nearly a pure isoscalar excitation. Recent ^{208}Pb $(\pi^{\pm}, \pi^{\pm})$ experiments[17] are also consistent with our result for the 3_1^- state. A calculation by Hamamoto[20] gives a value of $\tilde{M}_n/\tilde{M}_p = 1.06$, close to our value of 1.12(3).

The two 5^- states of ^{208}Pb are seen to be somewhat different in their neutron/proton ratios, the 5_1^- state being the more strongly neutron dominated. This is qualitatively similar to the results of random-phase approximation (RPA) calculations by Ring and Speth[21] and the earlier work of True, Ma, and Pinkston,[22] and Gillet, Greer, and Sanderson,[23] in which the largest component (amplitude ~ 0.88) of the 5_1^- (3.20) state is the $(2g_{9/2}, 3p_{1/2}{}^{-1})$ neutron configuration, while the 5_2^- (3.71) is more mixed in both neutron and proton particle-hole components. Similarly, the 2_1^+ and 4_1^+ states show, in the RPA calculations,[21,23,24] a large (> 0.8) neutron $(2g_{9/2}, i_{13/2}{}^{-1})$ amplitude in qualitative agreement with our results.

In the case of ^{90}Zr the four lowest collective states (2_1^+, 3_1^-, 4_1^+, and 5_1^-) all show $\tilde{M}_n/\tilde{M}_p \simeq 0.8$, while the 2_2^+ and 2_3^+ states appear to be more neutronlike. The 6_1^+ and 8_1^+ states, on the other hand, are strongly proton dominated, as expected in the simple shell model, in which these states are made by a recoupling of the $1g_{9/2}$ protons. The values of M_n/M_p obtained here for the 2^+ states of ^{58}Ni, ^{90}Zr, and ^{120}Sn are in fairly good agreement with those calculated from the one-parameter schematic model (OPSM) of core polarization by Brown and Madsen.[25] However, the M_n/M_p value for the 2_1^+ of ^{144}Sm is somewhat higher than that of the (OPSM) but equal to the N/Z ratio of the simple collective model. Full microscopic calculations are now being made for ^{90}Zr and ^{208}Pb to examine the quantitative agreement with current structure calculations.

We feel that this work demonstrates that the comparison of intermediate energy proton scattering with electromagnetic excitation is, at present, the most reliable method for obtaining the neutron-proton (or isoscalar-isovector) decomposition of transition matrix elements. The reasons for this are (1) the near equality of the 800 MeV proton potential and matter densities due to the short range of the N-N force, (2) the strong absorption, which justifies the use of surface peaked transition densities, and (3) the excellent fits to the data using these densities in the DWBA. The most serious limitation of the method at present seems to be the accuracy of the electromagnetic determination of $B(E\lambda)$. In cases for which several measurements exist the differences are frequently considerably greater than the quoted errors (Table IV).

A more sophisticated approach to the analysis of the proton data would be to take model independent proton transition densities from electron scattering, and then to search on the neutron densities with a fully microscopic reaction theory [distorted-wave impulse approximation (DWIA)] to fit the (p,p') data, in a manner analogous to that used in the determination of ground state densities from elastic scattering data.[13]

An independent method for the isoscalar-isovector decomposition of densities is the comparison of π^+ with π^- scattering in the vicinity of the 3-3 resonance. This method has roughly the same sensitivity to neutron-proton differences as the electron-proton comparison but at present is more difficult experimentally for reasons of energy resolution and beam intensity. However, the $(\pi^{\pm}, \pi^{\pm'})$ experiments should be pursued to check the consistency of both methods.

Note added in proof. A recent calculation by L. Ray (private communication) indicates that the inclusion of spin-orbit terms in both the diagonal and off-diagonal potentials would result in a potential deformation length 9—10% lower than that obtained here for the 8_1^+ state of ^{208}Pb.

ACKNOWLEDGMENTS

We are greatly indebted to the MP-10 staff at LAMPF, particularly H. A. Thiessen, for their continuous assistance during this experiment. We also wish to thank Rodger Liljestrand and Carol Harvey for their help during data taking. This research was supported by the U. S. Department of Energy.

*Present address: SIN, CH-5234 Villigen, Switzerland.
†Present address: University of South Carolina, Columbia, South Carolina 29208.

[1]See, for example, S. Iverson *et al.,* Phys. Lett 82B, 51 (1979); C. Olmer *et al.,* Phys. Rev. C 21, 254 (1980): D. F. Geesaman *et al., ibid.* 23, 2653 (1981); K. Boyer *et al., ibid.* 24, 598 (1981).
[2]See, for example, L. Ray, W. R. Coker, and G. W. Hoffmann, Phys. Rev. C 18, 2641 (1978).
[3]L. E. Smith, private communication.
[4]G. W. Hoffmann *et al.,* Phys. Rev. C 21, 1488 (1980).
[5]Modified version of program RAROMP by G. Pyle (unpublished).
[6]A. Bohr and B. R. Mottelson, *Nuclear Structure* (Benjamin, New York, 1975), Vol. II, p. 341 ff.
[7]Coupled channels program CHUCK by P. D. Kunz, modified by L. D. Rickertsen.
[8]G. S. Adams *et al.,* Phys. Rev. C 21, 2485 (1980).
[9]G. S. Kyle *et al.,* Phys. Lett. 91B, 353 (1980).
[10]V. A. Madsen, V. R. Brown, and J. D. Anderson, Phys. Rev. C 12, 1205 (1975); Phys. Rev. Lett. 34, 1398 (1975). See also A. M. Bernstein, V. R. Brown, and V. A. Madsen, Phys. Lett. 71B, 48 (1977) Phys. Lett. 103B, 255 (1981); A. M. Bernstein, *ibid.* 29B, 332 (1969); 29B, 335 (1969).
[11]G. R. Satchler, J. Math. Phys. 13, 1118 (1972).
[12]W. G. Love and M. A. Franey, Phys. Rev. C 24, 1073 (1981).
[13]L. Ray, Phys. Rev. C 19, 1855 (1979).
[14]Mainly from C. W. de Jager, H. de Vries, and C. de Vries, At. Data Nucl. Data Tables 14, 479 (1974). See also references in Table IV.
[15]L. Ray, Phys. Lett. 102B, 88 (1981); private communication.
[16]L. Ray *et al.,* Phys. Lett. 83B, 275 (1979).
[17]C. Olmer *et al.,* Phys. Rev. C 21, 254 (1980).
[18]C. L. Morris *et al.,* Phys. Rev. C 24, 231 (1981); private communication.
[19]A. M. Bernstein, Phys. Lett. 29B, 335 (1969).
[20]I. Hamamoto, Phys. Lett. 66B, 410 (1977); private communication.
[21]P. Ring and J. Speth, Nucl. Phys. A235, 315 (1974).
[22]W. True, C. W. Ma, and W. T. Pinkston, Phys. Rev. C 3, 2421 (1971).
[23]V. Gillet, A. M. Green, and E. A. Sanderson, Nucl. Phys. 88, 321 (1966).
[24]E. Weber, W. Knüpfer, E. Grecksch, and M. Huber, Phys. Lett. 65B, 189 (1976).
[25]V. R. Brown and V. A. Madsen, Phys. Rev. C 11, 1298 (1975). See also A. M. Bernstein, V. R. Brown, and V. A. Madsen, Phys. Lett. 71B, 48 (1977).